Results on hybrid control of self-oscillating resonant converters

Nicola Zaupa, Luis Martínez-Salamero, Carlos Olalla, Luca Zaccarian

Results on hybrid control of self-oscillating resonant converters ⋆

Nicola Zaupa * **Luis Martínez-Salamero** ** **Carlos Olalla** **
Luca Zaccarian *,***

* *Department of Industrial Engineering, Università di Trento, Italy*
** *Department of Electrical, Electronic, and Automatic Control Engineering, Universitat Rovira i Virgili, Tarragona, Spain*
*** *LAAS-CNRS, Université de Toulouse, CNRS, France*

Abstract: A unified set of input-dependent coordinates is proposed for the description of parallel and series resonant converters. The description naturally leads to a hybrid feedback control strategy for self-oscillating behavior. We show through a hybrid representation that the ensuing dynamics admits a unique almost globally attractive hybrid limit cycle. A tuning parameter, the switching angle, is then numerically shown to lead to monotonic variation of the peak output current/voltage and of the self-induced switching frequency. Numerical simulations with high-accuracy software illustrate the desirable behavior of the self-oscillating scheme, and it robustness to unmodeled phenomena.

Keywords: Hybrid dynamical systems, Resonant converters, Power electronics, Energy systems

1. INTRODUCTION

Resonant power conversion is of interest in different industrial applications, such as inductive heating and battery charging Lucía et al. (2010); Park and Choi (2014), thanks to its numerous advantages, including soft-switching and a high power density.

The typical resonant converters control approaches, which include frequency and amplitude modulation, exhibit nonlinear control-to-output characteristics, which complicate the control design. As an alternative, state-plane control approaches, where the switching decision is based on the current and voltage measurements in the converter, can streamline the design of a controller. The advantageous features of state-plane approaches have been well illustrated in the initial works Molla-Ahmadian et al. (2012, 2015), and then further developed in Bonache-Samaniego et al. (2016); Afshang et al. (2016); El Aroudi et al. (2019). Nonetheless, state-plane approaches also pose problems: typical assumptions include needing a resonant tank of sufficiently high quality factor Q, so that the controller can sustain the currents and voltages oscillation Bonache-Samaniego et al. (2016); El Aroudi et al. (2019).

In recent years, switching control of power electronics has been successfully cast as a design problem for so-called hybrid dynamical systems, wherein the dynamical state both involves physical quantities (voltages, currents) taking values in the reals and logical quantities (position of switches) taking values in the integers. Hybrid dynamics well capture the interplay between the continuous-time current/voltage evolution (wherein the logical states remain constant), and the discrete-time instantaneous changes of the logical states (with the physical states remaining unchanged across jumps). In particular, the powerful Lyapunov tools developed in Goebel et al. (2012) recently allowed to address several interesting power electronics challenges, such as the hybrid control of inverters in Chai and Sanfelice (2014); Torquati et al. (2017) and the hybrid control of DC-DC converters in Theunisse et al. (2015); Albea-Sanchez et al. (2019); Sferlazza et al. (2019), in addition to quadratic boost converters in Sferlazza et al. (2020).

In this paper, a novel unifying input-dependent coordinate transformation is proposed to analyze parallel and series resonant converters. The advantage is that the transformed dynamics, for both architectures, is described by the same hybrid equations, thus unifying the analysis. These hybrid equations naturally suggest a specific state-plane feedback control law, to ensure a self-oscillating closed-loop steady state. We prove here, for certain parameters selections, that the results in Bisoffi et al. (2016) prove almost global attractivity of a unique nontrivial limit cycle, associated to the desired resonant output. The specific oscillation amplitude and frequency can be adjusted using a single parameter that describes the switching surface in the newly proposed input-dependent set of coordinates. In the paper we also investigate the output voltage or current and frequency, as a function the control parameter, numerically showing that it has a monotonic behavior. Finally, we briefly address possible issues emerging with analog or digital implementations.

The structure of the paper follows. The proposed set of coordinates is given in Section 2 and the related hybrid system is introduced in Section 3. Sections 4 and 5 discusses the existence of a unique hybrid limit cycle whose amplitude and frequency can be adjusted using a tuning parameter. A possible digital implementation is discussed in Section 6. Final considerations and future directions are reported in Section 7.

Notation. $\mathbb{R}$ and $\mathbb{Z}$ denote, respectively, the sets of real and integer numbers. $\mathbb{R}_{>0}$ ($\mathbb{R}_{\geq 0}$) and $\mathbb{Z}_{>0}$ ($\mathbb{Z}_{\geq 0}$) denote,

⋆ Research supported in part by the University of Trento, via the international mobility plan, and by ANR via grant HANDY, number ANR-18-CE40-0010.

respectively the positive (non-negative) real and integer numbers. $\mathbb{R}^n$ denotes the Euclidean space of dimension $n \in \mathbb{Z}_{>0}$. Given two vectors $u \in \mathbb{R}^n$ and $w \in \mathbb{R}^m$, $u^\top$ denotes the transpose of u, and $(u, w) := \begin{bmatrix} u^\top & w^\top \end{bmatrix}^\top$. Given a (continuous, discrete, or hybrid) signal x, $\dot{x}$ denotes its derivative with respect to continuous time t, while x^+ denotes its next value with respect to discrete time j.

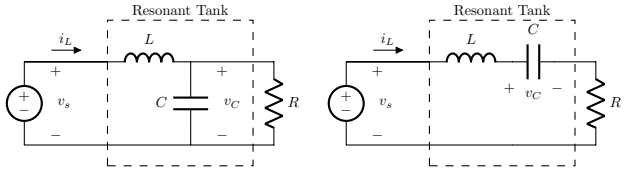

Fig. 1. Equivalent circuits of the parallel (PRC, left) and series (SRC, right) resonant converters.

2. UNIFYING COORDINATE CHANGE

Consider the two circuits of Fig. 1 and denote by v_C the voltage across the capacitor and by i_L the current flowing in the inductor. Assume that one of the two circuits be the resonant tank driven by a H-bridge capable of applying a voltage equal to either V_g or $-V_g$ to the supply voltage v_s applied to the left terminal. In particular, we consider a binary variable $\sigma \in \{-1, 1\}$ describing the switch position, so that $v_s = V_g$ when $\sigma = 1$ and $v_s = -V_g$ when $\sigma = -1$ (in summary $v_s = \sigma V_g$).

The linear equations governing the parallel configuration at the left of Fig. 1 are the following ones:

$$L\frac{\mathrm{d}i_L}{\mathrm{d}t} = \sigma V_g - v_C; \quad C\frac{\mathrm{d}v_C}{\mathrm{d}t} = i_L - \frac{v_C}{R}. \tag{1}$$

Similarly, the linear equations governing the series configuration at the right of Fig. 1 correspond to

$$L\frac{\mathrm{d}i_L}{\mathrm{d}t} = \sigma V_g - v_C - Ri_L; \quad C\frac{\mathrm{d}v_C}{\mathrm{d}t} = i_L. \tag{2}$$

Let us now introduce the next input-dependent quantities for the parallel case of (1):

$$\beta := \frac{1}{RC},\ z_1 := \frac{v_C}{V_g} - \sigma;\ z_2 := \frac{1}{V_g}\sqrt{\frac{L}{C}}\left(i_L - \frac{v_C}{R}\right), \tag{3}$$

where $\beta > 0$ is the inverse of the time constant of the exponential decay associated with the linear circuit, and we emphasize that the last term in brackets, $\left(i_L - \frac{v_C}{R}\right)$, is the current flowing in the capacitor, i_C. As a consequence, one can well think about these coordinates as z_1 being a transformed voltage and z_2 being a transformed current.

Let us also introduce the next input-dependent alternative coordinates for the series configuration in (2):

$$\beta := \frac{R}{L},\ z_1 := \frac{v_C}{V_g} - \sigma,\ z_2 := \frac{1}{V_g}\sqrt{\frac{L}{C}}i_L, \tag{4}$$

where $\beta > 0$ is once again the inverse of the time constant of the exponential decay associated with the linear circuit. Also here z_1 coincides with the previous case and represents a voltage, while z_2 is a current.

Keeping in mind that any variation of $\sigma \in \{-1, 1\}$ must be instantaneous, so that $\dot{\sigma} = 0$, we may compute the differential equations governing the evolution of variables $z := (z_1, z_2)$ in (3) (using dynamics (1)), and also those of the variables $z := (z_1, z_2)$ in (4) (using dynamics (2)). Notably, the two evolutions are exactly the same and correspond to the following damped oscillator

$$\dot{z}_1 = \omega z_2, \quad \dot{z}_2 = -\omega z_1 - \beta z_2 \tag{5}$$

where $\omega := \left(\sqrt{LC}\right)^{-1}$ is the characteristic frequency of both linear circuits.

With these definitions, we may also characterize the instantaneous updates of the new coordinates (z_1, z_2) and of the input σ whenever the switch of the converter changes position. Notably, since z_1 are exactly the same in (3) and (4), and z_2 never depends on σ, then we find the same instantaneous update for both circuits:

$$(z_1^+, z_2^+, \sigma^+) = (z_1 + 2\sigma, z_2, -\sigma), \tag{6}$$

where we emphasize that σ represents the switch position before the update and σ^+ represents its position after the update (and similarly for the other variables).

3. HYBRID MODEL AND SWITCHING LAW

The following unified dynamics represents both the parallel and series resonant converters, where we recall that $z = (z_1, z_2) \in \mathbb{R}^2$ is a physical state related to the current and voltage in the circuit, and $\sigma \in \{-1, 1\}$ is a logical state representing the position of the switch:

$$\begin{bmatrix} \dot{z} \\ \dot{\sigma} \end{bmatrix} = f(z, \sigma) := \begin{bmatrix} A_F z \\ 0 \end{bmatrix} \qquad (z, \sigma) \in \mathcal{C}(\theta) \tag{7a}$$

$$\begin{bmatrix} z^+ \\ \sigma^+ \end{bmatrix} = g(z, \sigma) := \begin{bmatrix} z + \begin{bmatrix} 2\sigma \\ 0 \end{bmatrix} \\ -\sigma \end{bmatrix} \qquad (z, \sigma) \in \mathcal{D}(\theta), \tag{7b}$$

where $A_F := \left[\begin{smallmatrix} 0 & \omega \\ -\omega & -\beta \end{smallmatrix}\right]$, $\omega > 0$ is the natural frequency and $\beta > 0$ is the internal dissipation.

The sets $\mathcal{C}$ and $\mathcal{D}$ in (7) are called, respectively, "flow set" and "jump set" and are subsets of $\mathbb{R}^2 \times \{-1, 1\}$ whose intuitive meaning is that whenever the (augmented) state $\xi := (z, \sigma)$ belongs to $\mathcal{D}$, it is time to change the switch position in the H-bridge driving the converter, whereas as long as $\xi \in \mathcal{C}$, one may let the converter evolve continuously without changing the switch position. We design below $\mathcal{C}$ and $\mathcal{D}$, parametrized by a so-called "switching angle" $\theta \in (0, \pi]$, representing a tuning knob of the proposed hybrid controller.

Following similar ideas to those in Bonache-Samaniego et al. (2017), select the jump and the flow sets as

$$\begin{aligned} \mathcal{C}(\theta) &:= \mathcal{C}_1(\theta) \cup \mathcal{C}_{\text{-}1}(\theta), \\ \mathcal{D}(\theta) &:= \mathcal{D}_1(\theta) \cup \mathcal{D}_{\text{-}1}(\theta), \end{aligned} \tag{8}$$

In selection (8), each set $\mathcal{C}_1(\theta)$ and $\mathcal{C}_{\text{-}1}(\theta)$ denotes a half plane and $\mathcal{D}_1$ and $\mathcal{D}_{\text{-}1}$ are two half lines at the boundary of $\mathcal{C}_1(\theta)$ and $\mathcal{C}_{\text{-}1}(\theta)$, namely

$$\mathcal{C}_q(\theta) := \{(z, \sigma) :\ \sigma = q, \sigma(z_1 \sin\theta + z_2 \cos\theta) \leq 0\}, \tag{9}$$

$$\mathcal{D}_q(\theta) := \{(z, \sigma) :\ \sigma = q, \sigma z_2 \geq 0, z_1 \sin\theta + z_2 \cos\theta = 0\}, \tag{10}$$

for $q \in \{1, \text{-}1\}$.

The rationale behind the switching mechanism captured by (8) is illustrated in Fig. 2, where two possible trajectories are shown by projecting the three-dimensional state-space (z_1, z_2, σ) on the "phase plane" (z_1, z_2) (voltage, current). The left figure represents the case $\theta < \frac{\pi}{2}$ while the right figure corresponds to $\theta > \frac{\pi}{2}$. During flowing (in $\mathcal{C}(\theta)$), the continuous evolution revolves in the clockwise

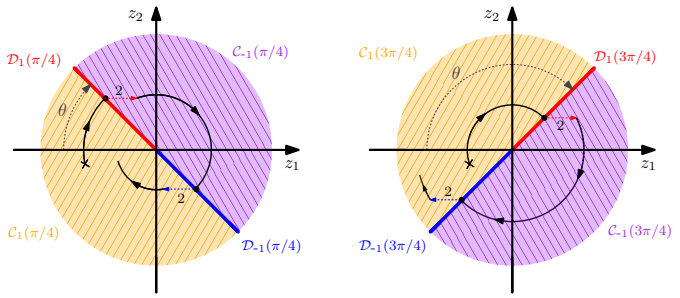

Fig. 2. Projection on the phase plane (z_1, z_2) of two possible solutions of system (7), (8) with $\theta < \frac{\pi}{2}$ (left) and $\theta > \frac{\pi}{2}$ (right).

direction. Switching always occurs when the continuous motion hits the tilted solid line. When a switch occurs, the z_1 voltage is shifted horizontally by two units, and the specific choice of $\mathcal{C}(\theta)$ and $\mathcal{D}(\theta)$ ensures that shifts always provide a clockwise rotation. The choice to split $\mathcal{D}$ in two half lines regularizes the domain avoiding Zeno solutions with $\theta = \pi$. With this choice, after a solution jumps, it is forced to flow because it never lands again into the jump set. The angle θ controls the tilting of the blue-red line, namely the subspace where the switch takes place. It is apparent that with small values of θ (left case in Fig. 2) solutions are forced to jump "earlier" when starting from the same initial condition.

Selection (8) provides a feedback control law. Indeed, checking whether or not the converter input should switch amounts to checking whether the state $\xi = (z, \sigma)$ belongs to $\mathcal{D}(\theta)$ or not. We show here that this feedback induces a self-oscillating behavior in the closed loop (7), (8).

4. EXISTENCE OF A LIMIT CYCLE

We study below the asymptotic behavior of solutions of the closed loop (7), (8). The notion of periodicity for a hybrid trajectory is a straightforward extension of the usual notion of periodicity.

Definition 1. (Bisoffi et al. (2016)) Given a hybrid system $\mathcal{H} = (\mathcal{C}, f, \mathcal{D}, g)$, a *hybrid periodic trajectory* is a complete solution ξ (namely a solution that evolves forever) for which there exist a pair (T, J) with either $T \in \mathbb{R}_{\geq 0}$ and $J \in \mathbb{Z}_{>0}$ or $T \in \mathbb{R}_{>0}$ and $J \in \mathbb{Z}_{\geq 0}$ such that $(t, j) \in \mathrm{dom}(\xi)$ implies $(t + T, j + J) \in \mathrm{dom}(\xi)$ and, moreover,

$$\xi(t, j) = \xi(t + T, j + J) \tag{11}$$

The image of ξ is a *hybrid periodic orbit*.

The following assumption on the parameters of the hybrid system (7) ensures the existence of a non trivial hybrid periodic trajectory. It intuitively means that the solutions of the flow dynamics revolve in the phase plane (z_1, z_2).

Assumption 1. Parameters ω and β are strictly positive reals. Moreover, the relation $\beta < 2\omega$ is satisfied, namely the resonant tank is underdamped. Equivalently, the roots of $s^2 + \beta s + \omega^2 = 0$ are complex conjugate.

Remark 1. Assumption 1 imposes constraints on the physical components to ensure that a natural oscillatory motion occurs. For the two considered circuit configurations these constraints correspond to:

$$PRC: \ 2R > \sqrt{\frac{L}{C}} \qquad SRC: \ \frac{R}{2} < \sqrt{\frac{L}{C}}. \tag{12}$$

This means that the damping induced by R must be sufficiently small to not destroy the natural oscillatory behavior of the LC network. Ideally, $R \to \infty$ (open circuit) for the PRC and $R \to 0$ (short circuit) for the SRC. ∘

The next theorem provides a justification for the proposed self-oscillating control law for the case $\theta = \frac{\pi}{2}$. Numerical test suggest that the result is true for any $\theta \in (0, \pi]$, but the proof is regarded as future work.

Theorem 1. Under Assumption 1, when $\theta = \frac{\pi}{2}$, the closed loop (7), (8) has a unique nontrivial hybrid periodic orbit $\mathcal{O}_\theta$ such that

(i) the orbit $\mathcal{O}_\theta$ is stable and almost globally attractive with basin of attraction corresponding to all points such that $z \neq 0$;
(ii) the unique nontrivial hybrid periodic solution of (7), (8) (the hybrid limit cycle) exhibits periodic jumps.

Proof. The proof of item (i) exploits the result in (Bisoffi et al., 2016, Thms 1+2). To this end, consider the coordinate change

$$x_1 := z_1, \quad x_2 := \omega z_2 \tag{13}$$

Using coordinates $x := (x_1, x_2)$, hybrid system (7) with $\theta = \frac{\pi}{2}$ can be rewritten as [1]

$$\begin{bmatrix} \dot{x}_1 \\ \dot{x}_2 \\ \dot{\sigma} \end{bmatrix} = \bar{f}(x, \sigma) := \begin{bmatrix} x_2 \\ -\beta x_2 - \omega^2 x_1 \\ 0 \end{bmatrix} \quad (x, \sigma) \in \bar{\mathcal{C}} \tag{14a}$$

$$\begin{bmatrix} x_1^+ \\ x_2^+ \\ \sigma^+ \end{bmatrix} = \bar{g}(x, \sigma) := \begin{bmatrix} 2\sigma \\ x_2 \\ -\sigma \end{bmatrix} \quad (x, \sigma) \in \bar{\mathcal{D}} \tag{14b}$$

$$\begin{aligned} \bar{\mathcal{C}} &:= (\bar{\mathcal{C}}_1 \times \{1\}) \cup (\bar{\mathcal{C}}_{\text{-}1} \times \{\text{-}1\}), \\ \bar{\mathcal{D}} &:= (\bar{\mathcal{D}}_1 \times \{1\}) \cup (\bar{\mathcal{D}}_{\text{-}1} \times \{\text{-}1\}), \end{aligned} \tag{14c}$$

with the four sets $\bar{\mathcal{C}}_1$, $\bar{\mathcal{C}}_{\text{-}1}$, $\bar{\mathcal{D}}_1$, $\bar{\mathcal{D}}_{\text{-}1}$ given by

$$\bar{\mathcal{C}}_q := \{x : q x_1 \leq 0\}, \qquad q = 1, \text{-}1, \tag{14d}$$

$$\bar{\mathcal{D}}_q := \{x : q x_2 \geq 0, x_1 = 0\}, \qquad q = 1, \text{-}1. \tag{14e}$$

The x subsystem of dynamics (14) coincides with (Bisoffi et al., 2016, eqn. (2)) for suitable values of the parameters of Bisoffi et al. (2016). For example, we may choose $m = 1$, $k = \omega^2$ and $\beta = c$ in (Bisoffi et al., 2016, eqn. (2)). Moreover, (Bisoffi et al., 2016, As. 1) is implied by our Assumption 1. As a consequence, we may apply Theorems 1 and 2 in Bisoffi et al. (2016) to prove the existence of a unique almost globally attractive hybrid orbit. Finally, item (ii) trivially follows from the fact that any periodic solution must exhibit periodic jumps due to the central symmetric of both the jump and flow dynamics, with respect to the origin. ■

Remark 2. The switching law induced by (8) is inspired by the one in Bonache-Samaniego et al. (2017) but differs from it in a few substantial ways. Among other things, for the parallel converter case, a nontrivial discussion is present in Bonache-Samaniego et al. (2016) characterizing what parameter selections lead to the self-oscillating feature, showing that when the quality factor $Q := \omega RC$ is too small, no oscillating behavior emerges by that switching law, and the converter reaches an (undesired) equilibrium. On the contrary, item (i) above proves that

[1] Recall that θ is a constant parameter and that $\dot{\theta} = 0$, not to be confused with the constant parameter $\omega = \left(\sqrt{LC}\right)^{-1}$.

the new switching law arising from the novel coordinates z proposed here always provides a self-oscillating behavior under Assumption 1, which is less restrictive. ○

Remark 3. The flow and jump sets of hybrid dynamics (7), (8) are closed, and the flow and jump maps are continuous functions, therefore, (7), (8) enjoys the so-called hybrid basic conditions of (Goebel et al., 2012, As. 6.5). This, among other things, implies robustness of asymptotic stability of compact attractors, as well characterized in (Goebel et al., 2012, Ch. 7). A consequence of robustness is that small perturbations of the system parameters (or of the jump triggering law, as in a digital implementation) cause a graceful performance degradation (the so-called semiglobal practical property). This robustness property is important for the controller implementation discussed in Section 6. ○

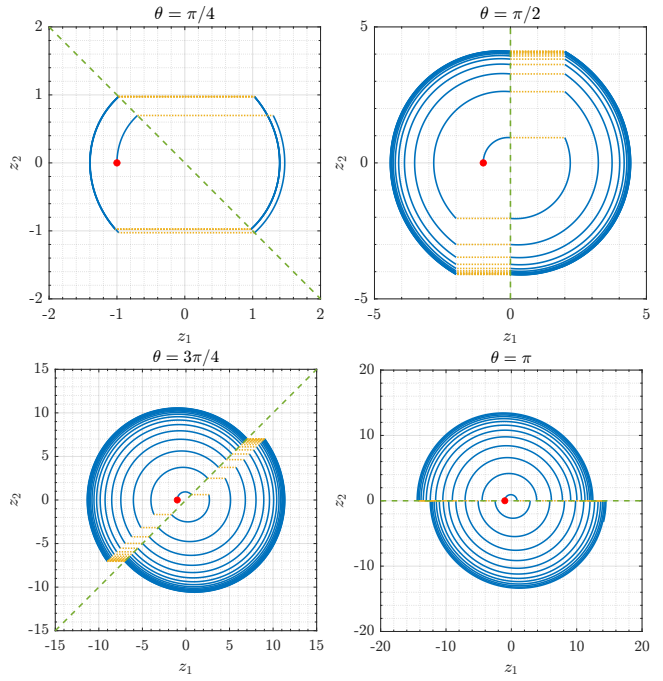

Fig. 3. Example 1: phase portrait with different values of θ. The θ-tilted dashed green line is the jumps set.

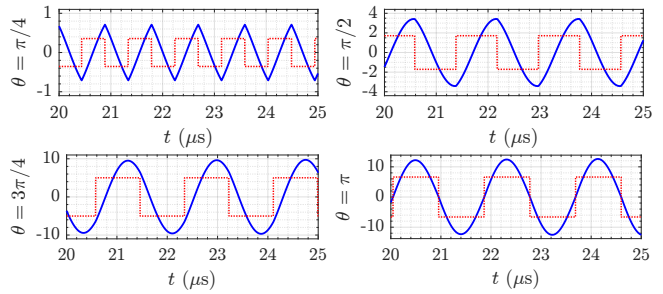

Fig. 4. Inductor current (blue line) and scaled version of the input voltage v_s (red line) from the hybrid simulations at the values of θ shown in Figure 3.

Example 1. Theorem 1 is illustrated here through numerical simulations of a PRC. The simulations are performed in MATLAB/Simulink using the *Hybrid Equations Toolbox* by Ricardo Sanfelice (2017). The physical parameters for the PRC are those of Bonache-Samaniego et al. (2016):

$$R = 400\,\Omega, \quad L = 8\,\mu\text{H}, \quad C = 10.5\,\text{nF}, \quad V_g = 20\,\text{V}. \tag{15}$$

Fig. 3 reports some phase plane trajectories in the coordinates z, showing the different behaviors for various values of θ. For small values of θ, the hybrid limit cycle evolves close to the horizontal axis and only flows for a small amount of time. By increasing θ, the flowing intervals become longer, up to the upper limit $\theta = \pi$, where the limit cycle spans all the phases while flowing. From Fig. 4, note that by increasing θ, the switching frequency decreases, while the amplitude of the steady-state oscillation increases, as characterized in the next section. The amplitude increase can be associated with the fact that the frequency is approaching the resonant frequency ω. ⋆

5. EFFECT OF PARAMETER θ

The previous section illustrates the existence of an almost globally attractive hybrid limit cycle for any $\theta \in (0, \pi]$ (and Theorem 1 proves this for $\theta = \frac{\pi}{2}$). Following Example 1, we may characterize the amplitude of this oscillation as a function of the control knob θ, as established in the next conjecture. Its proof is regarded as future work and may include explicit characterizations of the amplitude and frequency as a function of the control knob θ. While here, we provide a validation through numerical simulations. The aim is to analyze the influence of the control parameter θ. This characterization is useful for closing an outer feedback loop to regulate the output peak-to-peak voltage or current.

Conjecture 1. Under Assumption 1 for each selection of $\theta \in (0, \pi]$, there exists an almost globally asymptotically stable hybrid limit cycle. Moreover,

(i) the periodic evolution of z_1 (voltage) along the limit cycle has amplitude 1 when $\theta = 0$ and is strictly increasing with θ;
(ii) the periodic evolution of z_2 (current) along the limit cycle has zero amplitude when $\theta = 0$ and is strictly increasing with θ;
(iii) the frequency of the limit cycle becomes arbitrarily large as θ approaches zero (namely it approaches a purely discrete solution), and is strictly decreasing as θ increases.

In the parallel resonant converter case, by the definition of z_1, item (i) in Conjecture 1 implies that the output voltage v_C measured across the resistor R has zero amplitude with $\theta = 0^+$ and strictly increasing amplitude as θ increases. Instead, in the series resonant converter case, by the definition of z_1, item (ii) in Conjecture 1 implies that the output current i_L (which is proportional to z_2 from (4)) has zero amplitude when $\theta = 0^+$ and strictly increasing amplitude as θ increases.

Example 2. Using the same setup as in Example 1, the influence of θ on the frequency and the amplitude of the hybrid limit cycle is explored in the range $(0, \pi]$. In accordance with the sampled evolutions of Fig. 4, Fig. 5 confirms the statements of Conjecture 1. In particular, at the bottom of Fig. 5 the monotonic behavior of the states z_1 and z_2 is confirmed. At the top left of Fig. 5, the frequency approaches the resonant one (dashed line), corresponding to $\frac{1}{2\pi}\omega$, as θ tends to π. Moreover, as θ tends to zero, the frequency blows up to infinity.

The top right of Fig. 5 shows the phase shift between the input current and the input voltage, which tends to zero as the frequency tends to the resonant one, as

expected (pure resistive behavior and maximum power transmitted). These phase shifts match well the angle of the input impedance Z_{in}, computed as:

$$Z_{in}(\jmath\omega) = R\frac{1-\omega^2 LC+\jmath\omega L/R}{1+\jmath\omega RC}. \qquad (16)$$

and transformed into the corresponding dependence on θ by numerically inverting the relation between θ and the frequency ω, reported on the top left chart of Fig. 5.

These results confirm that the amplitude and frequency are nonlinear functions of θ. This has implications on the design of an outer control loop to stabilize a desired operating point. With a nonlinear relation, a solution can be to invert it in order to linearize the feedback and then use a simple PI control loop. The inverse relations, obtained by polynomially fitting the inverse results, are reported in Fig. 5 as solid red lines. ⋆

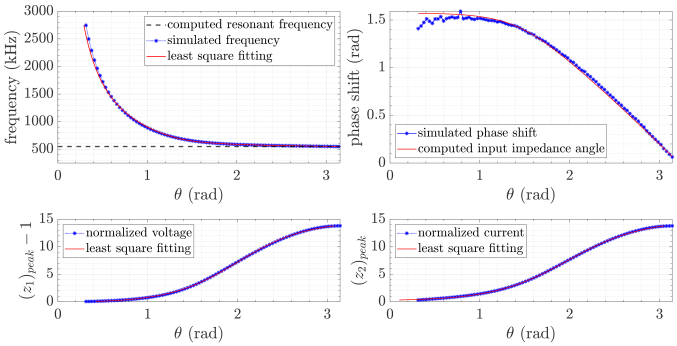

Fig. 5. Top left: frequency of the periodic trajectory, the dashed line represents the resonance frequency of the system. Top right: phase shift between the inductor current and the input voltage. Bottom: amplitude of the normalized PRC output voltage z_1 (left) and of the normalized SRC output current z_2 (right).

6. HIGH FIDELITY SIMULATION

For the practical implementation, through suitable measurements, it is necessary to gather enough information to understand whether the current state $z = (z_1, z_2)$ is in $\mathcal{C}$ or $\mathcal{D}$. If it is in $\mathcal{D}$, then a switch of σ must be performed. We show here that a direct measurement of $z = (z_1, z_2)$ is not strictly necessary and that, as long as the characteristic parameter $\sqrt{L/C}$ is known (in addition to the internal state σ), there is no need to measure any quantity in the load. In particular, as shown in the schemes of Fig. 6 and 7, it is enough to measure any scaled version (by an unknown factor $\mu > 0$) of the following electrical quantities accessible in the resonant tank, regardless of the PRC (3) or SRC (4) architecture of the converter:

$$y_1 = \mu v_C, \quad y_2 = \mu i_C, \quad y_3 = \mu V_g. \qquad (17)$$

Note that the above measurements are the scaled voltage and current on the capacitor, in addition to the constant scaled supply μV_g. Due to the sinusoidal waveforms characterizing the resonant tank, all of these measurements can be regarded as slowly varying, hence not much distortion is expected in the measurements due to possible filtering actions from the acquisition stage. Note also that i_C corresponds to the output current in the SRC and v_C to the output voltage in the PRC. Therefore, the measurements above provide enough information in order to close an outer loop for voltage/current regulation.

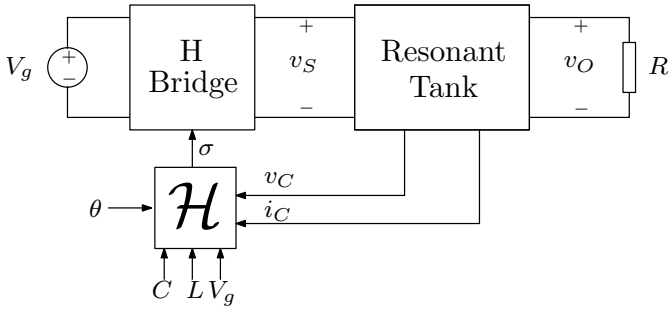

Fig. 6. Block diagram at sensing level with the electronic blocks and the controller $\mathcal{H}$.

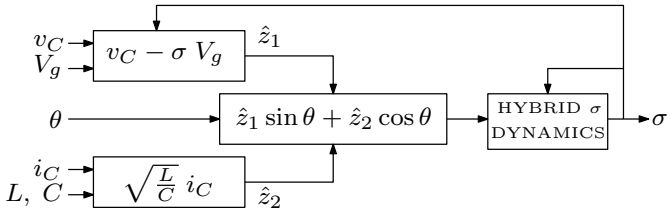

Fig. 7. Internal connections of block $\mathcal{H}$ in Fig. 6.

With the measurements in (17), we may define the following quantities:

$$\hat{z}_1 = y_1 - \sigma y_3 = \mu(v_C - V_g\sigma),$$
$$\hat{z}_2 = \sqrt{\frac{L}{C}}y_2 = \mu\sqrt{\frac{L}{C}}i_C,$$

and the expressions of $\mathcal{C}_q$ and $\mathcal{D}_q$ in (9) and (10) can be equivalently written as

$$\mathcal{C}_q(\theta) := \{(z,\sigma) : \ \sigma = q, \sigma(\hat{z}_1\sin\theta + \hat{z}_2\cos\theta) \le 0\},$$
$$\mathcal{D}_q(\theta) := \{(z,\sigma) : \ \sigma = q, \sigma\hat{z}_2 \ge 0, \hat{z}_1\sin\theta + \hat{z}_2\cos\theta = 0\}.$$

The above-described implementation has been tested by simulation in the power electronics design and circuit & system level simulation software PSIM, which accounts for accurate descriptions of the electrical components. The simulated circuit corresponds to an analog implementation of the proposed hybrid control scheme. When using the parameters in (15) (see Example 1), the resulting responses are indistinguishable from the plots reported in Figures 3 and 4, therefore they are not reported here.

A further simulation-based investigation has been performed to test, via PSIM, the real-time control architecture implementing a digital implementation of the control scheme. Digital implementations are more desirable in the early prototyping phases, because analog control requires cumbersome tuning/calibration for the circuit parameters, while digital control is more flexible.

On the other side, digital control does not provide a continuous monitoring of the switching conditions but only real-time sampled versions causing undesirable delays (mostly related to the sampling), thereby introducing nonuniform output evolutions. Although the robustness result in Remark 3 indicates that some level of delay is tolerable with an expected graceful degradation of the closed-loop properties, the sampling frequency should be kept sufficiently high (i.e. the delay low) within the limits of the required computational time for the processor to evaluate the control algorithm. For the simulated digital implementation, we report in Fig. 8 sampled-data results with $\theta = 3\pi/4$ for a relatively low frequency converter operating at a natural

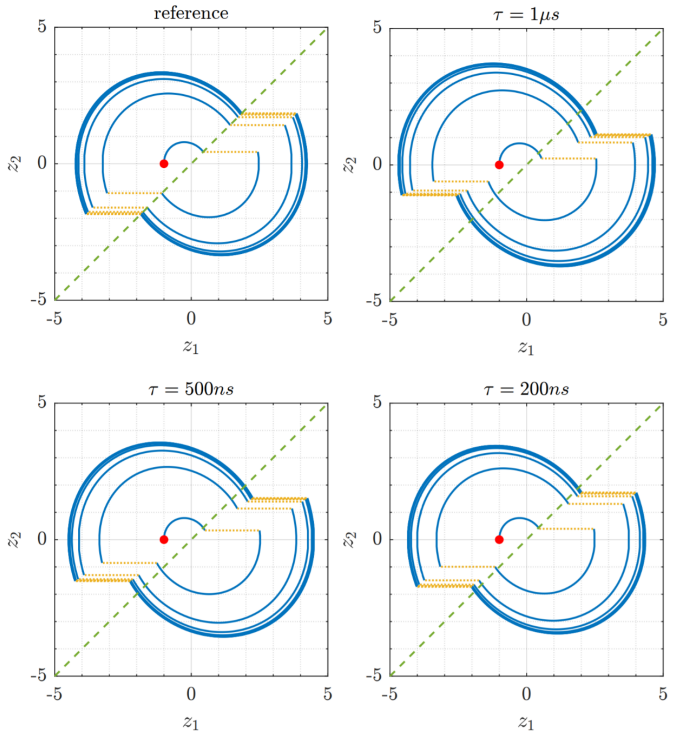

Fig. 8. Using $\theta = 3\pi/4$, analog implementation (top-left) and sampled-data implementation (remaining traces) with different sampling frequencies f_s.

frequency $\frac{1}{2\pi}\omega$ of 50 kHz, which allows having a reasonable amount of samples in a period with sampling frequency in the MHz range. More specifically, with the parameters $R = 100\,\Omega$, $L = 101\,\mu$H, $C = 100\,$nF, $V_g = 24\,$V, we first perform an analog simulation (the ideal behavior) reported at the top left of Fig. 8 (a half period of the cycle lasts about 10 µs). Then, real-time implementations with delays $\tau = 1\,$µs, $\tau = 500\,$ns and $\tau = 200\,$ns are reported in the remaining subfigures. We can observe in Fig. 8 the significant influence of the delay on the solutions.

7. CONCLUSIONS AND FUTURE DIRECTIONS

We proposed a unifying coordinate representation for PRC and SRC resonant converters, which led to a natural feedback control law, inducing an almost globally attractive hybrid limit cycle in a self-oscillating resonant behavior. With the proposed controller, the limit cycle emerges in underdamped conditions for any switching angle $\theta \in (0, \pi]$, providing a large range of output amplitudes and frequencies, whose trends, as a function of θ, have been characterized. Additionally, the influence of the control knob θ on the output evolution has been numerically characterized. This characterization provides an initial step towards closing a feedback loop for the regulation of the output voltage or current.

REFERENCES

Afshang, H., Tahami, F., and Mollaahmadian, H. (2016). Hybrid control of the dc-dc series resonant converter operating below resonance. *IET Power Electronics*, 10.

Albea-Sanchez, C., Garcia, G., Hadjeras, S., Heemels, W., and Zaccarian, L. (2019). Practical stabilisation of switched affine systems with dwell-time guarantees. *IEEE Trans. on Automatic Control*, 64(11), 4811–4817.

Bisoffi, A., Forni, F., Da Lio, M., and Zaccarian, L. (2016). Global results on reset-induced periodic trajectories of planar systems. In *European Control Conference*, 2644–2649.

Bonache-Samaniego, R., Olalla, C., and Martínez-Salamero, L. (2017). Dynamic modeling and control of self-oscillating parallel resonant converters based on a variable structure systems approach. *IEEE Transactions on Power Electronics*, 32(2), 1469–1480.

Bonache-Samaniego, R., Olalla, C., Martínez-Salamero, L., and Valderrama-Blavi, H. (2016). Design of self-oscillating resonant converters based on a variable structure systems approach. *IET Power Electronics*, 9(1), 111–119.

Chai, J. and Sanfelice, R. (2014). A robust hybrid control algorithm for a single-phase DC/AC inverter with variable input voltage. In *Proc. of the 2014 American Control Conference*, 1420–1425.

El Aroudi, A., Benadero, L., Ponce, E., Olalla, C., Torres, F., and Martinez-Salamero, L. (2019). Suppression of undesired attractors in a self-oscillating h-bridge parallel resonant converters under zero current switching control. *IEEE Transactions on Circuits and Systems II: Express Briefs*, 66(4).

Goebel, R., Sanfelice, R., and Teel, A. (2012). *Hybrid Dynamical Systems: modeling, stability, and robustness*. Princeton University Press.

Lucía, O., Burdío, J.M., Millán, I., Acero, J., and Barragán, L.A. (2010). Efficiency-oriented design of zvs half-bridge series resonant inverter with variable frequency duty cycle control. *IEEE Transactions on Power Electronics*, 25(7).

Molla-Ahmadian, H., Karimpour, A., Pariz, N., and Tahami, F. (2012). Hybrid modeling of a dc-dc series resonant converter: Direct piecewise affine approach. *IEEE Transactions on Circuits and Systems I: Regular Papers*, 59(12).

Molla-Ahmadian, H., Tahami, F., Karimpour, A., and Pariz, N. (2015). Hybrid control of dc–dc series resonant converters: The direct piecewise affine approach. *IEEE Transactions on Power Electronics*, 30(3).

Park, J. and Choi, S. (2014). Design and control of a bidirectional resonant dc–dc converter for automotive engine/battery hybrid power generators. *IEEE Transactions on Power Electronics*, 29(7).

Ricardo Sanfelice (2017). Hybrid equations toolbox v2.04. `https://www.mathworks.com/matlabcentral/fileexchange/41372-hybrid-equations-toolbox-v2-04`.

Sferlazza, A., Albea-Sanchez, C., and Garcia, G. (2020). A hybrid control strategy for quadratic boost converters with inductor currents estimation. *Control Engineering Practice*, 103, 104602.

Sferlazza, A., Albea-Sanchez, C., Martínez-Salamero, L., Garcia, G., and Alonso, C. (2019). Min-type control strategy of a dc–dc synchronous boost converter. *IEEE Trans. on Industrial Electronics*, 67(4), 3167–3179.

Theunisse, T.A., Chai, J., Sanfelice, R., and Heemels, W. (2015). Robust global stabilization of the DC-DC boost converter via hybrid control. *IEEE Trans. on Circuits and Systems I: Regular Papers*, 62(4), 1052–1061.

Torquati, L., Sanfelice, R., and Zaccarian, L. (2017). A hybrid predictive control algorithm for tracking in a single-phase DC/AC inverter. In *IEEE Conference on Control Technology and Applications*, 904–909. Kohala Coast (HI), USA.